Deuterium retention in tungsten irradiated by different ions

B. Wielunska[1,2], M. Mayer[1], T. Schwarz-Selinger[1], A. E. Sand[3], W. Jacob[1]

[1]Max–Planck–Institut für Plasmaphysik, Boltzmannstr.2,

85748 Garching, Germany

[2]Physik-Department E28, Technische Universität München,

James-Franck-Strasse 1,85748 Garching, Germany

[3]Department of Physics, University of Helsinki, P.O. Box 43, FI-00014, Helsinki, Finland

Abstract

Tungsten was irradiated with different ion species (H, D, He, Si, Fe, Cu, W) at energies between 0.3 and 20.3 MeV to two different calculated damage levels of 0.04 dpa and 0.5 dpa. Samples were exposed to a low-temperature deuterium (D) plasma at 370 K to decorate the radiation defects. D retention was studied by nuclear reaction analysis using the D(^{3}He, p)α reaction and by thermal desorption spectroscopy. For tungsten irradiated by light ions (H, D, He) the depth profiles as well as D desorption spectra show clear differences. On the other hand, tungsten irradiated by medium- to high-mass ions (Si, Cu, Fe, W) to identical dpa values shows similar D depth profiles and nearly identical D desorption spectra, i.e., the D retention is comparable. Since

the large differences in the primary recoil energy distribution due to different incident energies of the different ions (Si, Cu, Fe, W) do not result in a different D retention, we assume that neutron irradiation of tungsten in a future fusion reactor will result in a similar D retention as in tungsten damaged by medium- to high-mass ions. Irradiation with ions with a mass of 28 amu (Si) or higher seems to be a suitable proxy for investigating the influence of displacement damage by neutrons on D retention.

1 Introduction

Tungsten is a promising plasma-facing material due to its low sputtering yield, high melting temperature and low hydrogen retention [1, 2]. In a future fusion device tungsten will be exposed to high fluxes of energetic deuterium and tritium ions, atoms and molecules as well as to high fluxes of 14 MeV neutrons from the DT-fusion reaction. This neutron irradiation will produce defects in the tungsten lattice which can trap hydrogen isotopes. The hydrogen retention of displacement-damaged tungsten is increased by orders of magnitude compared with the undamaged material [3, 4, 5]. For radiation safety it is important to keep the T retention as low as possible. For example in ITER the total in-vessel T inventory should be kept below 700 g [6]. Understanding the hydrogen isotopes retention in neutron-irradiated tungsten is, therefore, a key issue for the safe operation of future fusion devices.

Unfortunately, a high flux 14 MeV neutron source is not yet available. Fission neutrons have a significantly different energy spectrum with an average energy

of < 2 MeV. Therefore, they can be used only to a certain extent to investigate the neutron irradiation in a future fusion reactor. Moreover, experiments with tungsten irradiated by fission neutrons are typically difficult to conduct because of the long exposure times in the reactor and the long cooling-down times due to activation of the samples. Additionally, such reactor irradiations are often not well defined in terms of temperature and dose rate [7].

Ion irradiation is comparatively fast inducing only little or no radioactivity. Different ion species with keV - MeV energies are used to simulate fusion neutron displacement damage in tungsten. According to [8, 9, 10] heavy ions are a good proxy for simulating displacement damage caused by neutrons as they generate dense collision cascades with large defect clusters which is also typical for neutron irradiation. For hydrogen isotopes retention studies ion irradiation has been used for many years to create displacement damage in tungsten [3, 4, 5, 11, 12, 13].

D retention in unirradiated or irradiated tungsten has been extensively studied. To create displacement damage, different ions at different energies were used. As a consequence, the primary tungsten recoil energy spectrum for the damage creation was different and can affect the damage distribution and, consequently, the D uptake in tungsten. Therefore, it is an open question to what extent the D retention in tungsten irradiated by different ions is comparable with each other and in how far these observations can be representative for the displacement damage neutrons will cause.

To address the first question of these two, tungsten was irradiated by different ions (H, D, He, Si, Fe, Cu and W) to damage levels of 0.04 dpa and 0.5 dpa. This ion irradiation produced displacement damage in tungsten. In the following work the

expression "damage" is used to describe "displacement damage". After decorating the produced defects with D from a low-temperature plasma the D retention in these samples was investigated using nuclear reaction analysis (D(^{3}He, p)α) and thermal desorption spectroscopy.

2 Damage Calculation

To investigate the D retention in tungsten irradiated by different ions (H, D, He, Si, Fe, Cu, W) a comparable thickness of the radiation damage zone, where the deuterium gets trapped, is favorable. With this a direct comparison of the D retention without additional scaling is possible. Therefore, the incident ion energies were chosen such that they always produce a damage zone of about 2 μm with a damage peak at around 1.5 μm. The incident ion energies were chosen based on calculations by SRIM 2008.04 [14]; the resulting different incident energies are listed in Tab. 1. The incident energies cover a wide energy interval from 0.35 MeV for H to 20.3 MeV for W irradiation. In order to characterize radiation damage, the displacement per atom (dpa) concept is widely used [15, 16]. The dpa value is the number of displaced atoms divided by the number of material atoms in the same volume. The dpa value indicates the level of irradiation exposure of the material. Nevertheless, it is important to remember that the dpa value is not equal to the actual defect concentration found in the material after irradiation [15]. Rather, defects in metals are in general fewer in number than the dpa value suggests, and additionally, they may be formed in clusters of different type. Subsequent processes such as recombination of Frenkel pairs or diffusion and agglomeration of interstitials or vacancies are not taken into account in the SRIM calculations [15].

For the dpa calculations SRIM was run for the different ion species at the given incident energies (Tab. 1) using the damage calculation mode "Ion Distribution and Quick Calculation of Damage" calculating 10^6 incident ions for each ion species. In this program mode the recoil/damage calculation uses the Kinchin-Pease model. A tungsten displacement threshold energy of 90 eV was used and the lattice binding energy was set to zero as recommended in [17]. The file vacancy.txt gives the calculated number of vacancies produced by the incident ions and the recoils [14].

Taking the number of vacancies from vacancy.txt the dpa value for a given irradiation fluence and vice versa was calculated with Eq. 1.

$$dpa(depth) = \frac{sum\,of\,vacancies\,per\,incident\,ion\,and\,depth\,intervall}{material\,density} \cdot fluence \quad (1)$$

This method of dpa calculation gives values comparable to the calculation method recommended by Stoller et al. [18]. All used dpa values in this paper are calculated in this way. Other works such as [4, 5, 19] used SRIM in the program mode "Detailed Calculation with full Damage Cascades" with a threshold energy of 90 eV giving around twice as large dpa values for 20.3 MeV self-damaged tungsten compared with the here used dpa values [18].

The damage depth profiles as calculated by SRIM for the different irradiations are shown in Fig. 1. The damage profiles have a damage peak at around 1.5 μm, as only one incident energy was used. The irradiation fluences given in Tab. 1 were calculated with Eq. 1 such that the values of 0.04 dpa and 0.5 dpa are reached at the damage peak maximum.

In the following text the different tungsten samples will be named after the

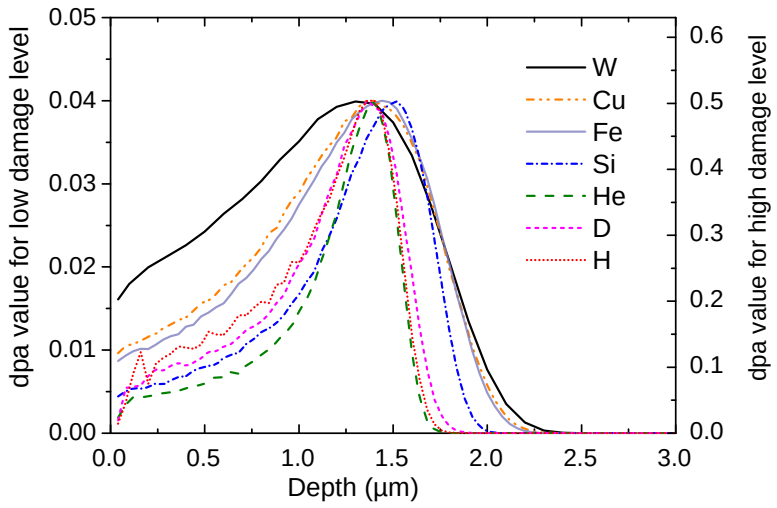

Figure 1: Calculated damage depth profiles in tungsten damaged by W, Cu, Si, Fe, He, D, H ions. Left y-axis: dpa value for damaging up to 0.04 dpa in damage peak maximum;
right y-axis: dpa value for damaging up to 0.5 dpa in damage peak maximum. Reproduced from [20] with permission.

ion they were irradiated with and the damage level in the peak maximum. For example the tungsten sample damaged by Cu up to 0.5 dpa is called Cu 0.5 dpa sample.

For self-damaged tungsten D retention is reported for different damage levels by several authors [4, 21, 19]. The D retention in self-damaged tungsten was observed to increase at low damage levels with dpa. It is expected to increase linearly at very low damage levels. At high damage level the D retention was observed to saturate. The absolute values of the D retention reported by the different authors are not easy to compare as they calculated the damage level in different ways and loaded the samples at different temperatures. We choose here to rely on the work of Ogorodnikova and Gann [21]. It is the most complete experimental series of different dpa values and the results coincide very well with recent experiments of us [22] which were performed with identical experimental parameters as applied in the present study in terms of W flux, W energy, and D loading temperature. According to our study [22] at around 0.2 dpa D retention is saturated, i.e., higher dpa values do not increase the local D retention further. In order to study the D retention behavior two different sets of samples were prepared. One set of samples was prepared at a high damage level to represent the saturation regime. To make sure that not only at the depth around the damage peak D retention saturation is reached, a damage level at the damage peak maximum of 0.5 dpa was chosen. The other set of samples was damaged up to 0.04 dpa in the damage peak maximum so that saturation in D retention should not yet set in. This damage level is high enough to study quantitavely the D retention in the sample. At this damage level the D retention is expected to still increase with dpa and to be close to the linear

regime expected for very low dpa. It represents the increase regime.

Figure 1 shows the damage depth profiles obtained from SRIM and illustrates the saturation behaviour in more detail. In the damage depth profile of W 0.5 dpa, one recognizes that throughout the whole damage zone the calculated damage level is higher than 0.2 dpa. That means that the D retention will reach the maximum possible local amount of D over the whole damage depth, i.e., it will be fully saturated. For the samples Fe 0.5 dpa and Cu 0.5 dpa the 0.2 dpa level is exceeded only in a depth larger than about 0.5 μm. Hence, local D saturation is only expected in the depth range from 0.5 μm to 1.9 μm. In the Si 0.5 dpa and He 0.5 dpa samples the 0.2 dpa level is exceeded between the depths of 1 μm and 1.8 μm. Hence, in this damage range local D retention saturation is expected. In the samples irradiated up to 0.04 dpa no D retention saturation effect is expected as throughout the whole damage zone the damage level is smaller than 0.2 dpa. Hence, the local D retention in the 0.04 dpa samples should roughly follow the damage depth profile. In Tab. 1 all ion species and their incident energies and fluences are listed. The amount of backscattered ions is in all irradiations <1% and, hence, negligible. That in turn means that all incident ions for damaging are implanted into the samples. Using different energies for obtaining a similar damage range unavoidably results in different recoil energy spectra because of the different incident ion energies and because of the different energy transfer due to differing ion masses. The recoil spectra, shown in Fig. 2, were calculated using MDRANGE [23], a molecular dynamics-based code for simulating energetic ions penetrating crystalline material. In MDRANGE, the interaction of the ion with atoms in the target material is described by the universal ZBL repulsive potential [24], and the ion trajectory

ion	incident energy (MeV)	max. energy of recoils (MeV)	fluence in ion/cm^2 corresponding to 0.04 dpa	fluence in ion/cm^2 corresponding to 0.5 dpa
W	20.3	20.3	$1.36\cdot 10^{13}$	$1.71\cdot 10^{14}$
Cu	9	6.9	$4.44\cdot 10^{13}$	$5.55\cdot 10^{14}$
Fe	9	6.4	$5.23\cdot 10^{13}$	$6.54\cdot 10^{14}$
Si	7.5	3.5	$1.34\cdot 10^{14}$	$1.68\cdot 10^{15}$
He	1	0.083	$5.00\cdot 10^{15}$	$6.25\cdot 10^{16}$
D	0.35	0.015	$2.72\cdot 10^{16}$	
H	0.35	0.0076	$7.96\cdot 10^{16}$	
n	14	0.3045		

Table 1: Irradiation parameters used in the presented experiments. Comparison with 14 MeV neutrons is shown in the last row.

is explicitly calculated by integrating the equations of motion as in regular molecular dynamics. Interactions between target atoms are disregarded, providing high computational efficiency while retaining the accuracy of full MD for calculations of energetic projectiles. Electronic stopping of the projectile is added as a friction force, the magnitude of which is taken from SRIM. For the heavy ions Fe, Cu and W, 10 000 ion trajectories were calculated, while for the lighter ions Si, He, D and H, which cause fewer energetic recoils and hence require more statistics, 100 000 trajectories were calculated. The obtained energy distributions of recoils were then scaled to the respective ion fluences used in this work for the 0.04 dpa samples (see column 3 in Tab. 1). The primary recoil energy distribution is then given per square cm through the whole implantation depth. Figure 2 shows the calculated primary recoil energy spectra in tungsten irradiated by the here used ions. Additionally shown is the primary recoil spectrum in tungsten under DEMO first-wall neutron irradiation as calculated by Gilbert et al. [25]. The vertical lines

mark the energy intervall between 42 eV and 90 eV. 42 eV is the experimentally determined lowest displacement energy in tungsten in the crystalographic direction $\langle 100 \rangle$ [26] and 90 eV is the displacement energy in tungsten recommended for use by ASTM [17]. Hence, for recoils with energies below this marked energy intervall no further damage production is expected. From Fig. 2 it can be seen that the primary recoil energy spectrum resulting from the irradiation with low mass ions (H, D, He) shows a steep decrease up to the highest possible recoil energy for the specific ion. A large fraction of these primary recoils has only a low energy and is, therefore, not able to produce further damage (energy range below the 2 vertical lines in Fig. 2). The irradiation with medium- to high-mass ions (Si, Fe, Cu, W) leads to primary recoil distributions which decrease not as steeply as for the light ions and extend to much higher maximal recoil energies. The primary recoil distribution for neutron irradiation under DEMO first-wall conditions is relatively flat over a large energy interval. The maximal recoil energy for the here applied ion irradiation conditions is listed in Tab. 1. These maximal recoil energies span a very wide range. While a 0.35 MeV proton can at most transfer 7.2 keV to a W atom, a 7.5 MeV Si produces recoils up to 3.5 MeV and 20.3 MeV W up to 20.3 MeV. The maximal recoil energy for 14 MeV neutrons is 290 keV and lies in the middle of the range covered here.

Different ions have a different damage efficiency, i.e., produce a different amount of displacements. Table 2 shows the calculated number of vacancies per incident ion separated into the damage created directly by the incident ions and the damage created by the recoils. It can be seen that for medium- to high-mass ions (Si, Fe, Cu, W) most of the radiation damage is produced by the recoils and not by the

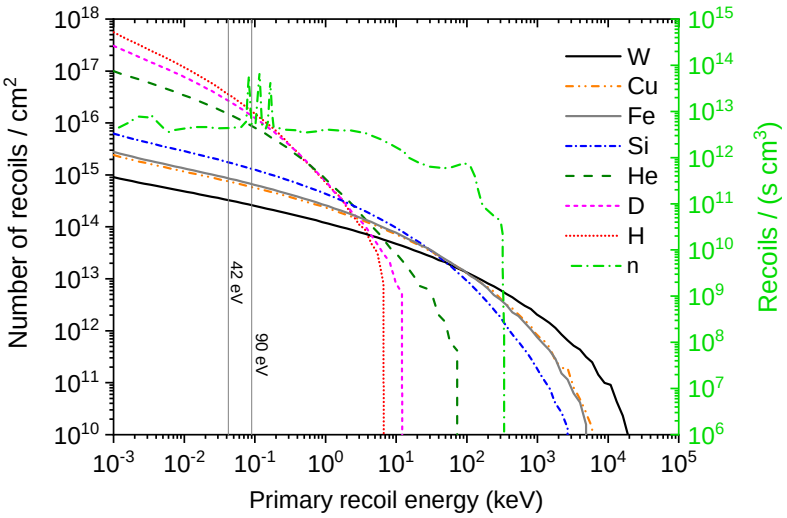

Figure 2: Primary recoil energy spectra for the 0.04 dpa irradiation for the different ions calculated by MDRANGE as described in the text. Additionally the primary recoil spectrum in tungsten calculated by Gilbert et al. [25] under DEMO hcpb (helium-cooled pebble-bed) first wall neutron irradiation is shown. The left y-axis refers to the ions and the right axis refers to the neutrons. Note please the different units. The vertical lines mark the displacement energy of 42 eV and 90 eV in tungsten.

incident ions itself. This situation is different for light ions (H, D, He). There the radiation damage originating from the incident ions is of the same order or even higher than the radiation damage due to the recoils. Due to technical reasons the ion current during the irradiations is different depending on the ion species used leading to different ion fluxes during the irradiation. In addition, due to the different damage efficiencies different irradiation fluences are needed to obtain the same dpa value in the damage peak. Therefore, not only the recoil energy spectra vary by more than three orders of magnitude, but also the average and peak damage rates (dpa/sec.) differ. The resulting average damage rates in the damage peak maximum are also listed in Tab. 2. Schwarz-Selinger [27] showed that a difference by a factor of 3 in the peak damage rate does not influence the D retention in self-damaged tungsten. In this work, however, the difference in the peak damage rate is up to about three orders of magnitude. Therefore, using different ions at different energies, it is possible to study the influence of the different primary recoil spectra and the different peak damage rates on the D retention.

In order to minimize chemical effects of the implanted ions on D retention, their concentrations should be low. Figure 3 shows the resulting maximum atomic percentages as a function of depth as calculated by SRIM [14]. The atomic percentage of the implanted ions ranges from 3 to 51 ppm in the damage peak maximum in the samples W 0.5 dpa, Cu 0.5 dpa, Fe 0.5 dpa and Si 0.5 dpa. In the samples irradiated with W, Si, Fe, Cu, Si up to 0.04 dpa the implanted ion amount is more than ten times smaller. It is assumed that such small impurity concentrations do not significantly influence the D retention behavior in tungsten, however, this can not be completely excluded [28]. In contrast, the irradiations with H, D, He result

ion	vacancies produced by ions	vacancies produced by recoils	vacancies in total	damage rate in $\frac{dpa}{s}$
W	0.036	1.82	1.86	$4.4{\cdot}10^{-5}$
Cu	0.029	0.54	0.57	$2.2{\cdot}10^{-4}$
Fe	0.028	0.46	0.48	$1.3{\cdot}10^{-4}$
Si	0.023	0.17	0.19	$6.7{\cdot}10^{-5}$
He	0.0031	0.0020	0.0051	$2.8{\cdot}10^{-6}$
D	$7.12{\cdot}\ 10^{-4}$	$2.21{\cdot}\ 10^{-4}$	$9.33{\cdot}\ 10^{-4}$	$1.1{\cdot}10^{-6}$
H	$2.74{\cdot}\ 10^{-4}$	$4.4{\cdot}\ 10^{-5}$	$3.18{\cdot}\ 10^{-4}$	$6.7{\cdot}10^{-7}$

Table 2: Calculated vacancies produced per incident ion in the damage peak maximum. The last column shows the experimentally obtained damage rate ($\frac{dpa}{s}$) for the different ions in the damage peak maximum.

in concentrations of the order of 0.5-4 at.% in the maximum. He bubbles in He-irradiated tungsten samples were observed [29, 30, 31]. Therefore, the formation of He bubbles has to be expected especially in the tungsten samples irradiated by helium up to 0.5 dpa since in that case the used fluence was $6.2{\cdot}10^{16}\ \frac{at}{cm^2}$. Also for hydrogen isotopes, bubble formation has to be taken into account. A threshold for blistering of tungsten implanted by keV H or D was reported to be between 10^{18}-$10^{19}\ \frac{at}{cm^2}$ [32, 33, 34]. It can be assumed that the blistering mechanism is strongly correlated with the preceding H bubble formation [32, 33, 34]. The here used energies in H and D irradiations were in the hundreds of keV energy range. The fluences for H and D were 0.8 and $0.3{\cdot}10^{17}\ \frac{at}{cm^2}$ and are, therefore, below the reported values for blistering. Although the H bubble formation cannot be completely ruled out for the H 0.04 dpa and D 0.04 dpa samples its possible influence on the here shown results is expected to be not significant.

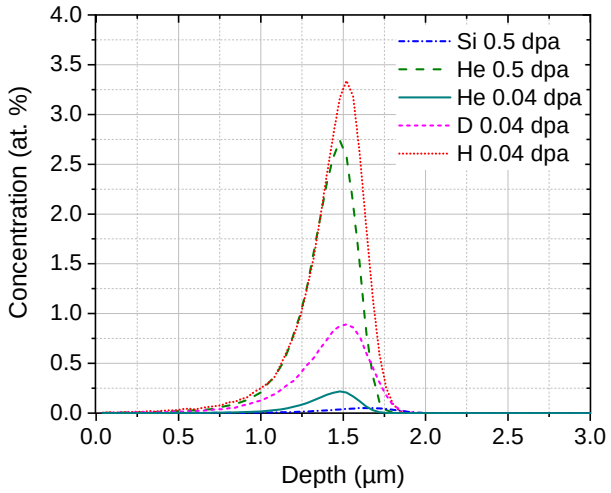

Figure 3: Implanted ion depth distributions for the samples Si0.5dpa, He0.5dpa, He0.04dpa, D0.04dpa and H0.04dpa as calculated by SRIM. The implanted ion concentration in the samples W0.5dpa, W0.04dpa, Cu0.5dpa, Cu0.04dpa Fe0.5dpa Fe0.04dpa and Si0.04dpa is of the order of 3-51ppm and hence would be not visible in the above image. The implated ion depth distribution data in logarithmic scale are available in the supplementary material. Reproduced from [20] with permission.

3 Experimental

Polycrystalline W samples of a size of 10 x 10 x 0.7 mm^3 and a purity of 99.97 wt.% from Plansee SE, Austria were used [35]. All samples were from the same manufacturing batch, i.e., the texture and purity of the samples was comparable. The samples were mechanically polished with a final grinding step of P2500 SiC paper as in [36] and then electro polished with 1.5 % NaOH at 19 V for 15 min to mirror-like finish. After polishing, the samples were outgassed at 1200 K in ultra high vacuum for 30 min. To reduce intrinsic defects and to anneal the distortions introduced by the polishing process the samples were annealed at 2000 K for 5 min by electron bombardement in an ultra high vacuum ($<10^{-5}$ Pa). After the recrystallization process the initial (as delivered) dislocation density of $2{\cdot}10^{12}m/m^3$ is reduced by about two orders of magnitude [37]. The grain size in the samples was measured to be between 10 to 30 μm in diameter.

The irradiations of the samples were performed at the TOF beamline of the 3 MV tandem accelerator of the Max-Planck-Institut für Plasmaphysik. During irradiation the samples were fixed with a molybdenum mask with an opening area of 8 x 8 mm^2 mounted on a water-cooled copper holder to prevent temperature rise of the sample. To measure the ion current during irradiation a water-cooled aperture with four faraday cups at the corners is placed in front of the sample holder. In order to damage the whole sample surface homogeneously and to measure the current with the faraday cups a focused ion beam of about 2 mm in diameter is scanned over the area of the front aperture and the faraday cups [27]. Due to this current measurement the ion flux incident on the sample can be calculated. The W irradiation was found in [27] to be homogeneous within 2%. Due to uncertain-

ties in the current measurement, the damage level is accurate within 10%. In the 0.5 dpa damage level this uncertainty should not make a large difference as the D retention is in any case far in the saturation regime, but for the 0.04 dpa damage level this uncertainty could slightly affect the D retention behavior.

To decorate the defects with D, samples were exposed to a low-temperature D plasma in the electron-cyclotron-resonance plasma source PlaQ [38]. The temperature of the samples during D loading was kept at 370 K. For the chosen pressure of 1 Pa the ion flux consists of 94% D_3^+ ions, 3% D_2^+ and 3% D^+[38] with a total D flux of 7.2 $\cdot 10^{19}$ $\frac{D}{m^2 s}$. The plasma potential of 15 eV results together with the applied dc-bias voltage of -10 V in a mean energy of 8 eV/D for the dominant ion species. It is important to note that these conditions were chosen such that no additional defects are created during the D loading as studied in detail in [39]. All samples damaged to the same dpa value were exposed to the deuterium plasma simultaneously. The D exposure time for the 0.5 dpa samples was 86 h and for the 0.04 dpa samples it was 48 h. The time was chosen based on preceding measurements to ensure the whole damaged zone to be D loaded [40]. As blisters can considerably enhance D retention [41], the surfaces of the loaded samples were investigated with the scanning electron microscope FEI Helios NanoLab 600 at IPP Garching. No blisters or cracks were found on the samples as expected for the chosen exposure paramters [39].

Nuclear reaction analysis (NRA) with D(^{3}He,p)α was conducted in the fourth week after the D loading to obtain the D depth profiles and the D amount in the damaged samples. A proton energy spectrum measured at a certain incident energy contains the information about the deuterium depth profile within the ^{3}He

ion range. To determine a deuterium depth profile with a reasonable depth resolution several different incident ^{3}He energies have to be used [42]. Eight different energies of the ^{3}He beam between 500 keV and 4500 keV were used to measure D depth profiles up to a depth of 7.4 μm. At each energy a nominal charge of 10 μC was accumulated. To obtain the depth profiles the measured proton and alpha spectra were used. The proton spectra were collected by two semiconductor detectors. One proton detector has a depletion depth of 2000 μm and a solid angle of 30.26 $\pm$ 1.18 msr and is located at the reaction angle of 135°. It will be called the small proton detector. The second proton detector has a larger solid angle and will be called large proton detector. It has a depletion depth of 3300 μm and a solid angle of 77.5 $\pm$ 3.0 msr. It is located also at 135°. In front of the proton detectors foils are installed to prevent backscattered ^{3}He ions from reaching the detectors. In front of the first proton detector a foil consisting of a 5 μm thick Ni layer and a 12 μm thick biaxially-oriented polyethylene terephthalate (BO-PET) foil coated with 10 nm Au is positioned. The Ni foil faces the target. In front of the large proton detector a foil consisting of a 50 nm Au layer and 50 μm BO-PET is installed. The alpha spectra are collected by a semiconductor detector with a depletion depth of 700 μm installed at 102° and a solid angle of 7.65$\pm$0.26 msr. A 3.5 μm BO-PET foil is installed in front of the detector to block the backscattered ^{3}He ions.

The detected energy spectra are a convolution of the deuterium depth distribution, the energy-dependent differential cross sections, the stopping powers in the elements and the experimental conditions such as the solid angle of the detector and number of incident ^{3}He ions. The determination of the deuterium depth pro-

files requires a simultaneous fitting of the simulated spectra by SIMNRA [43] to the measured energy spectra.

The deconvolution of the measured spectra was performed by the program NRADC as described in [44] using SIMNRA 7.01 as simulation kernel [43] to simulate the alpha and proton energy spectra. Additionally, at each ^{3}He energy a deuterated carbon thin film (a-C:D) sample was measured for energy calibration. Cross section data from [45] were used. Given the energy spectra, NRADC applies Bayesian statistics to find the most probable deuterium depth profile with the least amount of free parameters. The program first finds an optimum number of layers of constant concentration and then conducts a Markov Chain to find the best depth sampling and concentration describing the data. The maximum likelihood approach is applied to fit the experimental data to determine the confidence interval. This procedure gives then the most probable D depth profile. The user can define a minimum depth resolution with respect to depth within the Markov Chain sampling in the program. If the program calculates a layer thickness below this depth resolution this solution is rejected. To calculate the minimum depth resolution at a given depth ResolNRA was used [46]. The such determined D concentration depth profiles are step profiles. The step widths are due to the limited depth resolution of the nuclear reaction analysis method [42]. The steps are showing the average D concentration in a given depth interval. In a recent upgrade of NRADC a new method for calculating the statistical uncertainties was introduced. A detailed description can be found in [47, 48]. In this paper the D depth profiles in Fig. 7 are shown with their 3σ uncertainties calculated by this new method.

After the NRA analyses, thermal desorption spectroscopy was performed. The

samples were heated in the quartz tube of the TESS device [49] with a linear oven temperature ramp of 3 K/min from 300 K to 1100 K. During the heating ramp, the desorbed gases were analyzed by a quadrupole mass spectrometer [49]. The signals of mass channels 1, 2, 3, 4, 14, 16, 17, 18, 19, 20, 27, 28, 29, 32, 44 were recorded. It was assumed that only the irradiated area of the sample of 0.64 cm^2 (as a 8 x 8 mm^2 mask was used during ion irradiation) was contributing to the D desorption. As only the oven temperature is measured during the measurement and not the real sample temperature, a temperature calibration was executed after the measurement. For this a thermo-couple wire of type K was spot welded to a W sample of identical size and surface finish. The sample temperature was then recorded during an identical ramp. With this, the measured oven temperature could be correlated with the actual temperature of the sample.

Deuterium desorbs mainly as D_2 (mass channel 4) and HD (mass channel 3) with a small contribution of HDO (mass channel 19) and D_2O (mass channel 20). After each measurement a D_2 gas flow calibration was performed using a calibrated leak to relate the measured intensity to the actual deuterium flow. The calibration factor of HD was 66% from that derived for D_2 as described in detail in [50]. The deuterium desorption flux was determined by summing up the D amount from mass channels 3 and 4, after background substraction. The amount of D desorbed in form of HDO and D_2O was negligible for all here investigated samples.

4 Results

As D retention in irradiated tungsten was studied, the effect of long-term D outgassing after D loading in such a sample was also investigated. For this, a self-

damaged tungsten sample with 0.23 dpa was D loaded in PlaQ at 370 K for 72 h to load the whole damage zone. Nuclear reaction analysis was conducted after the D loading after $1, 3, 7, 23, 80, 296$ and 536 days. At each measurement day and after three incident energies a different measurement point on the sample was chosen to avoid ion-beam-driven D loss. Measurements with seven different ^{3}He energies ranging from 500 keV to 4.5 MeV were conducted. Figure 4 shows the integrated proton peak counts for all measured ^{3}He energies versus the days passed since the D exposure. A measurement uncertainty of up to 5 % was determined for every measurement point. This uncertainty is due to three reasons: 1. the uncertainty of the homogeneity of the sample is up to 3%. This was determined in a seperate measurement at 12 different points on the sample. 2. the uncertainties in the current measurement (estimated to be up to 3%) and 3. the counting statistics (the square root of the counts). A clear drop of the number of counts is observed during the first week. The reduction of counts continues up to about 80 days after D loading. After this time the outgassing effect continues only slowly. After 1.5 years from the D loading the counts in the proton peak decreased by about 15 % for the low energies 500 keV and 690 keV and 11-13 % for the medium incident energies 1200 keV, 1800 keV and 6-9 % for the high energies 2400, 3200, 4500 keV. This means a D outgassing effect is observed over the complete D containing depth and is strongest for the first 1 μm.

Having this effect in mind it is important to perform the nuclear reaction analysis for D depth profiling always in a comparable time interval after D loading. Therefore, nuclear reaction analysis with D(^{3}He,p)α and thermal desorption spectroscopy were always conducted in the fourth week after the D loading.

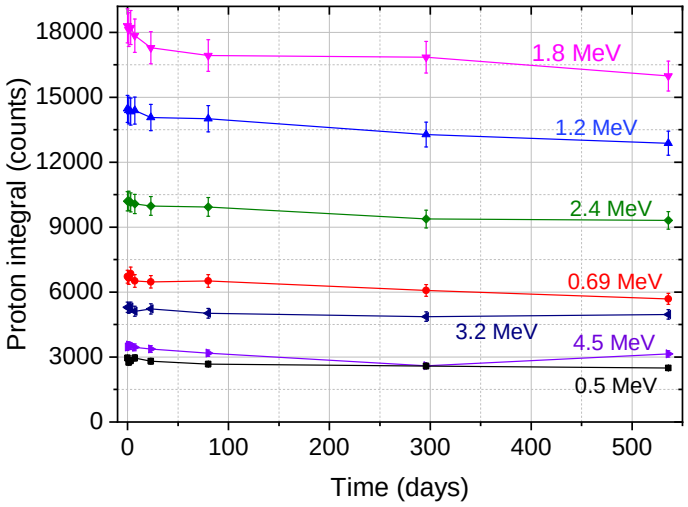

Figure 4: Integral counts in the proton peak for different incident ^{3}He energies versus time passed since D loading, measured with the large proton detector.

Figure 5 shows the total amounts of retained D for all damaged samples as measured by NRA and TDS. Additionally, the retained D amounts are listed in Tab. 3.

To obtain the total amount of D within the damage zone the depth profiles from NRA are integrated over depth. To derive the total amount of D degassed from the sample the calibrated D desorption spectra were integrated over time. A good agreement within 10 % between the two measurements is found for all samples showing that all D is retained within the damage zone. Retention in the recrystalized bulk beyond the damage zone can be neglected. To compare D retention in undamaged tungsten under the chosen plasma conditions one additional reference sample was exposed together with the self-damaged sample used for the long term outgassing study described before. The reference sample was from the same material batch, was also electro-polished, and annealed at 1200 K

for 0.5 h but was neither recrystallized nor irradiated with MeV ions. The total D amount of this unirradiated tungsten sample was also measured by NRA. It is about $2.7 \,\mathrm{x}\, 10^{15}\, \frac{at}{cm^2}$, and hence less than 1% of the D amount retained in the damaged samples, compare Tab. 3. Intrinsic defects, such as grain bounderies, and dislocations govern the D retention in unirradiated tungsten. In re-crystallized tungsten, these intrinsic defects are substantially reduced and hence D retention is lower [37, 51, 52]. We can therefore neglect in the following the influence of intrinsic defects in all irradiated samples of this study.

As described above D retention in self-damaged tungsten saturates at a damage level above 0.2 dpa [21, 19]. Hence, samples in which the damage level exceeds locally the 0.2 dpa level will show local D saturation. The 0.5 dpa samples were irradiated such to reach the 0.5 dpa level in the damage peak maximum. As discussed in Sect. 2, the W 0.5 dpa sample is expected to be fully D saturated as in the whole damage zone the local damage level is higher than 0.2 dpa, compare Fig. 1. Cu 0.5 dpa and Fe 0.5 dpa samples are expected to be close to full D saturation as they are expected to be locally D saturated in the depths from 0.5 μm to 1.8 μm as in this depth range the damage level is higher than 0.2 dpa (Fig.1). As the samples W 0.5 dpa, Cu 0.5 dpa and Fe 0.5 dpa are close to full D saturation they should retain a comparable amount of D. This is indeed the case. It can be seen in Fig. 5 that the total amount of D retained in W 0.5 dpa, Cu 0.5 dpa and Fe 0.5 dpa is comparable. In Sect. 2 it was already discussed that in the Si 0.5 dpa sample the 0.2 dpa level is exceeded only between the depths of 1 μm and 1.8 μm. At the surface its damage level is only about 0.1 dpa. Therefore, the Si 0.5 dpa sample was expected to be only locally D saturated for depths larger than 1 μm. Nev-

ertheless, the total amount of retained D in the Si 0.5 dpa sample is very similar to the samples W 0.5 dpa, Cu 0.5 dpa and Fe 0.5 dpa, therefore, it seems that the Si 0.5 dpa sample is also close to full D saturation. The total D amount retained in the He 0.5 dpa sample is significantly lower, meaning that this sample is not saturated with D. This is in agreement with the expectation, as in a large fraction of the damage zone the dpa value is significantly lower than 0.2 dpa.

All 0.04 dpa samples show a lower D retention. Although the damage level in the samples damaged up to 0.04 dpa is more than ten times smaller than for the 0.5 dpa samples, the D retention is only up to three to four times smaller (Fig. 5). This can be expected as the D retention saturates at higher dpa levels. When looking at the total amount of D retained in the 0.04 dpa samples in Fig. 5 it seems that the D amount retained in the sample is correlated with the damaging ion species. Since the 0.04 dpa damage level is in the increase regime, close to the linear regime of D retention, a higher local damage level results in a higher local D retention. The local damage level in the damage peak was for all samples 0.04 dpa, but the integrated damage over the full damage depth is different for the different samples, compare Figs. 6 and 1. Therefore, the raw data of the 0.04 dpa samples need to be normalized to the same integral damage to allow a meaningful comparison of the total D retention.

Figure 7 shows the measured D depth profiles determined by NRA together with the calculated SRIM damage profiles for all samples. The present version of NRADC allows to use only two different detectors. It was decided to use for the 0.5 dpa samples, the signals from the small proton detector at 135° and the α detector to have a very good depth resolution at the first 500 nm depth. In

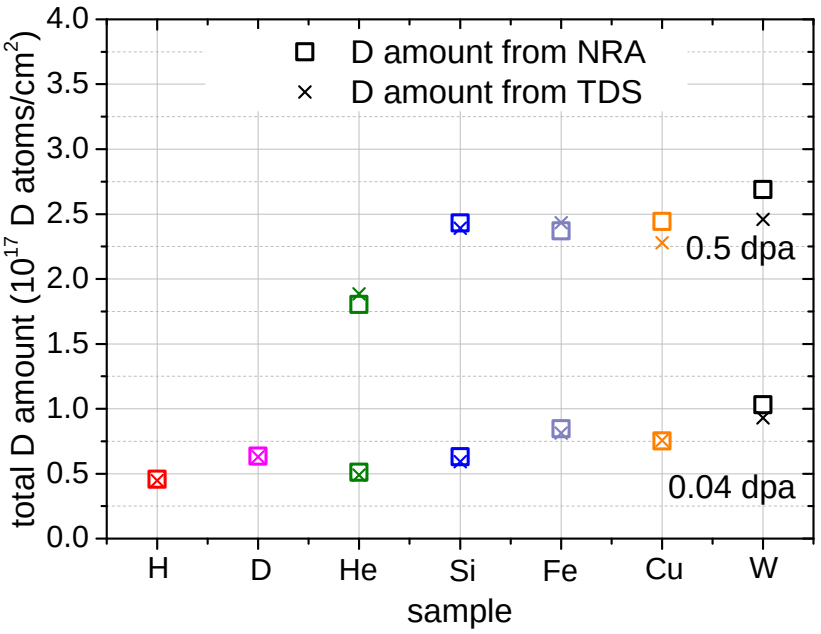

Figure 5: Total amounts of D retained in tungsten determined by NRA and TDS for different damaging ions. Reproduced from [20] with permission.

the 0.04 dpa samples the D concentration was expected to be lower and because of that it was important to have a good counting statistics. Therefore, the two available proton detectors at 135° were used. The D depth profiles are shown with their 3σ uncertainty determined by NRADC in the final Markov Chain Monte Carlo (MCMC) optimization. The D depth profiles of the 0.5 dpa samples show a higher D retention than the D depth profiles from the 0.04 dpa samples, as more trapping sites are available for D. For all measured samples the SRIM damage range is comparable to the D retention depth. From this, we conclude that all present defects were decorated with D indicating that the D loading time in PlaQ was chosen long enough.

Total D amount in 10^{17} at./cm^2				
0.5 dpa			0.04 dpa	
ion	NRA	TDS	NRA	TDS
W	2.69	2.46	1.03	0.93
Cu	2.44	2.28	0.75	0.76
Fe	2.37	2.43	0.85	0.81
Si	2.43	2.39	0.63	0.59
He	1.80	1.89	0.51	0.49
D			0.64	0.63
H			0.46	0.45

Table 3: Total D amount in 10^{17} at./cm^2 obtained by NRA and TDS for the 0.5 dpa and 0.04 dpa samples.

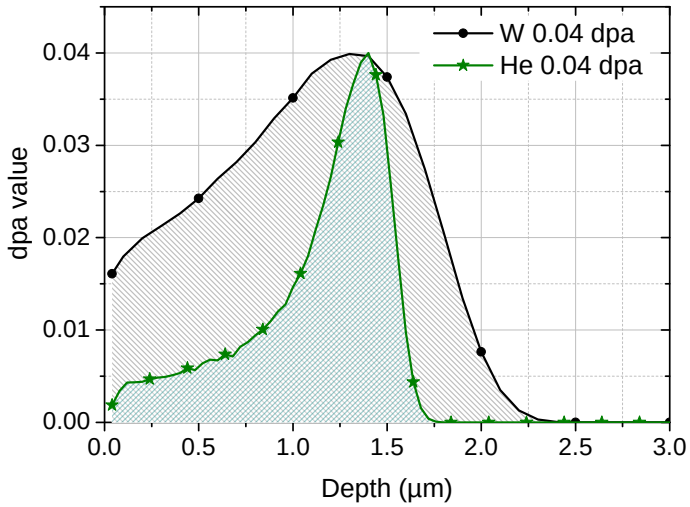

Figure 6: Damage depth profiles calculated by SRIM for samples W 0.04 dpa and He 0.04 dpa. Both damage depth profiles reach the 0.04 dpa level in the damage peak maximum. Nevertheless, the damage depth profiles' integrals are significantly different. The integrated damage depth profile of W 0.04 dpa is twice as large as the damage integral of He 0.04 dpa. Reproduced from [20] with permission.

First, the results of the irradiations up to 0.5 dpa will be discussed. The 0.2 dpa level above which D saturation is expected [21, 19] is shown as a red line in Fig. 7. As visible in Fig. 7 the maximum D concentration reached in W 0.5 dpa, Cu 0.5 dpa and Fe 0.5 dpa is 1.8 at.%. Si 0.5 dpa reaches a slightly higher D concentration of 2 at.%. In Fig. 7a it is visible that for self-damaged tungsten damaged up to 0.5 dpa (W 0.5 dpa sample) the damage level is higher than 0.2 dpa up to a depth of 1.8 μm. Therefore, the D depth profile of the W 0.5 dpa sample should be flat up to this depth, i.e., the maximum possible D amount is retained. The NRA D depth profile of W 0.5 dpa shows a D concentration of 1.8 at.% up to 1.4 μm and drops slightly to 1.6 at.% up to a depth of 2.2 μm. Taking into account the statistical uncertainties indicated by the thin lines in the D depth profiles and the limited depth resolution of the used NRA method it can be concluded that the W 0.5 dpa sample is saturated with D up to a depth of about 1.9 μm, as expected. Hence, full D saturation is reached. The Cu 0.5 dpa depth profile shown in Fig. 7b) is also almost flat. In the near surface layer up to a depth of 0.08 μm the D concentration is only 1.3 at.%. Then it rises to 1.8 at.% in the maximum up to a depth of 2 μm. The Fe 0.5 dpa sample depth profile (Fig. 7c)) shows from the surface to 0.22 μm a D concentration of 1.6 at.%. A maximal D concentration of 1.8 at.% is reached between 0.22 μm and 2 μm. As for W 0.5 dpa the D depth profiles of the Cu 0.5 dpa and Fe 0.5 dpa samples are almost flat and practically fully saturated with a maximum D concentration of 1.8 at.%. Comparing the D depth profiles with the calculated SRIM damage depth profiles in Fig. 7 it seems that the maximum D retention value is reached already at around 0.13-0.15 dpa and not only above 0.2 dpa, which is still in accordance with [21] as there is no data point between 0.14 dpa and 0.45 dpa.

From Fig. 1 it is seen that the Si damage depth profile reaches 0.13-0.15 dpa at a depth of about 0.7 μm. Hence, it can be expected that Si 0.5 dpa sample will be locally D saturated in the depth range between 0.7 μm and 1.8 μm, i.e., it will be close to full D saturation. The measured D concentration profile for Si 0.5 dpa increases from 1.2 at.% at the surface to 1.7 at.% up to a concentration of 2.0 at.% at the damage peak maximum (Fig. 7d)). Taking into account the uncertainties and remembering that the steps in the depth profiles are showing an average D concentration in a certain depth interval it can be concluded that indeed saturation is reached locally between 0.6 μm and 2 μm.

The D depth profile of the He 0.5 dpa sample is shown in Fig. 7e). This D depth profile is significantly different than those presented so far. The D concentration increases steeply from 0.9 at.% through 1.3 at.% up to 2.4 at.% at a depth of 0.8 μm and drops to 0.22 at.% from a depth of 1.5 μm up to a depth of 2.4μm. For all D depth profiles for 0.5 dpa the D-filled range is in good agreement with the damage depth range predicted by SRIM. Damaging up to 0.5 dpa was not conducted with H and D ions due to the excessive required damaging fluences, see Tab. 1. Figure 8 shows the D depth profiles for the samples damaged up to 0.5 dpa in one figure. Comparing the D depth profiles of W 0.5 dpa, Cu 0.5 dpa and Fe 0.5 dpa and taking into account their statistical uncertainties (3σ), it is obvious that they can be considered as being identical. D saturation is reached in the whole damage zone (beside the first 200 nm in Cu 0.5 dpa and Fe 0.5 dpa). Compared with these, the Si 0.5 dpa D depth profile is only locally saturated with a somewhat higher D concentration in the D peak maximum. Taking into account the statistical uncertainties shown in Fig. 8 and remembering that the steps are showing the average D

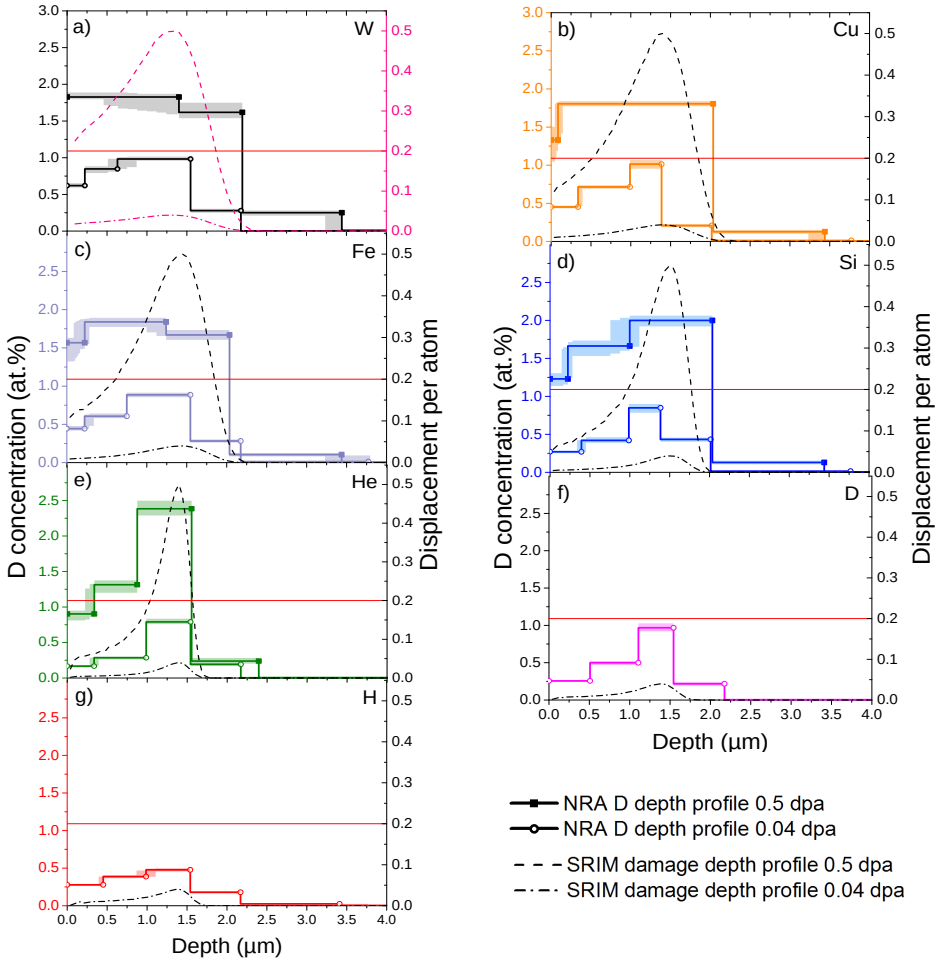

Figure 7: D depth profiles measured by NRA (step profiles) and SRIM calculated damage depth profiles (dashed lines) shown for all samples damaged with different ions (W, Cu, Fe, Si, He, D, H) at 0.04 dpa and 0.5 dpa. The colored areas are $3\,\sigma$ uncertainties. The damaging ion is denoted in the figure. The red lines indicates the 0.2 dpa level at which D retention saturation is reached. Reproduced from [20] with permission.

concentration in a given depth intervall it is clear that for the Si 0.05 dpa sample full D saturation is not reached, but its D depth profile is similar to the D depth

profiles of Fe 0.5 dpa, Cu 0.5 dpa and W 0.5 dpa.

The depth profile of the He 0.5 dpa sample is significantly different. The D concentration in the damage peak in He 0.5 dpa sample is up to 30 % higher compared with the W 0.5 dpa sample. The accumulation of D in the He-implantation region in tungsten was already reported by Markelj et al. [53]. It was shown that He attracts D and that D retention increases in the presence of He. This can be explained by He clustering or He bubble presence in the sample. MD simulations show that a large amount of H can be trapped around the He bubbles [54]. Hence, no D saturation effect was observed in the He 0.05 dpa sample.

Figure 9 shows the D desorption spectra for the same set of samples shown in

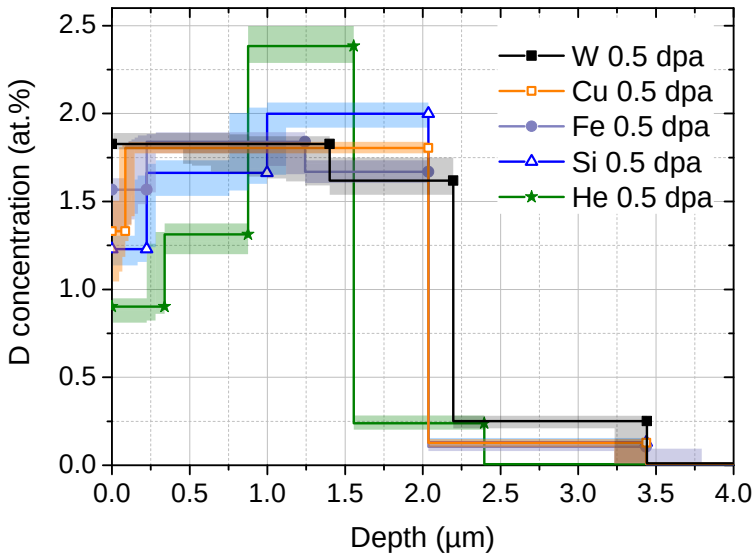

Figure 8: D depth profiles in tungsten irradiated by medium- to high-mass ions (Si, Fe, Cu, W) for 0.5 dpa. The uncertainty bands indicate the 3σ uncertainty. Reproduced from [20] with permission.

Fig. 8. All D desorption spectra consist of at least three peaks and start and end at identical temperatures. The first peak is located at about 490-500 K, the second one at about 590-600 K and the third one at about 770-780 K. In the samples W 0.5 dpa, Cu 0.5 dpa, Fe 0.5 dpa and Si 0.5 dpa the two first peaks are difficult to distinguish as they both merged into one broad peak structure. The third peak is clearly separated. The D desorption spectra of these three samples are almost identical. Only some small, not significant differences are discernible in the first broad peak structure. The third peak is identical. Si 0.5 dpa was found to be only locally D saturated in the depth range of 0.6 μm and 1.9 μm. Nevertheless, the D desorption spectrum of Si 0.5 dpa is very similar to the spectra of W 0.5 dpa, Cu 0.5 dpa, Fe 0.5 dpa. Therefore, it can be stated that Si 0.5 dpa is close to full D saturation. This allows the conclusion that the D retention is the same for medium- to high-mass ions in the 0.5 dpa case. In references [4, 5, 13, 55, 56] the peaks are assigned to represent D desorption from different defect types. The D desorption spectra of medium- to high-mass ions are nearly identical, i.e., the detrapping energies and intensities are nearly identical. With this it can be assumed that the defect structure is similar as well.

The D desorption spectrum obtained from the He 0.5 dpa sample is significantly different. The D desorption spectrum shows three well distinguishable peaks. The first peak is found at about 470 K, the second peak is seen at around 610 K and the third at about 730 K. All three peaks in the D desorption spectrum of He 0.5 dpa are found at slightly different temperatures than for medium- to high-mass ion samples. The second peak in the He 0.5 dpa D desorption spectrum is highest. This significantly different D desorption spectrum suggests that also a different

defect structure can be expected in tungsten damaged by He ions. The helium fluence during 1 MeV He irradiation of tungsten up to 0.5 dpa was $6.25{\cdot}10^{16}\ \frac{at}{cm^2}$. Using transmission electron microscopy Miyamoto et al. [29] observed nm sized He bubbles in tungsten after an exposure to 50 eV. Hashimoto et al. observed nanometric He bubbles in tungsten irradiated with 1.3 MeV He ions at 850°C at a fluence of $10^{15}\frac{at}{cm^2}$ and annealed at 2000°C [31]. Gilliam et al. [57] and Debelle et al. [58] found strong evidence from NRA studies for the existence of He bubbles in 1.3 MeV He implanted tungsten at fluences in the range of $10^{15} - 10^{18}\ \frac{at}{cm^2}$. In a different project, the He 0.5 dpa sample was investigated with respect to He bubbles and indeed He bubble candidates were found [59]. Therefore, He bubbles can be expected in the He 0.5 dpa and He 0.04 dpa samples. These nm size bubbles which are supposed to act as additional trapping sites for D are probably the explanation for the significant change in the D retention behavior of tungsten [53, 54].

Let us now discuss the D retention in the 0.04 dpa samples. Figure 7 shows also the D depth profiles for the samples damaged up to 0.04 dpa. The D depth profiles are not as flat as the D depth profiles from 0.5 dpa samples. This is well understandable as the maximum local damage level throughout the whole damage zone stays well below the damage saturation level of 0.13 - 0.15 dpa (see discussion above). For all samples the D retention range and the position of the maximum of the D retention are in reasonable agreement with the SRIM predictions, compare Figs. 7a)–7b). However for Si 0.04 dpa, Fe 0.04 dpa and Cu 0.04 dpa the maximum in the NRA depth profiles is located at slightly smaller depths than predicted by SRIM, Figs. 7 b), c), d). As expected from the SRIM damage depth profile the D depth profile of W 0.04 dpa shows the broadest maximum compared with the other

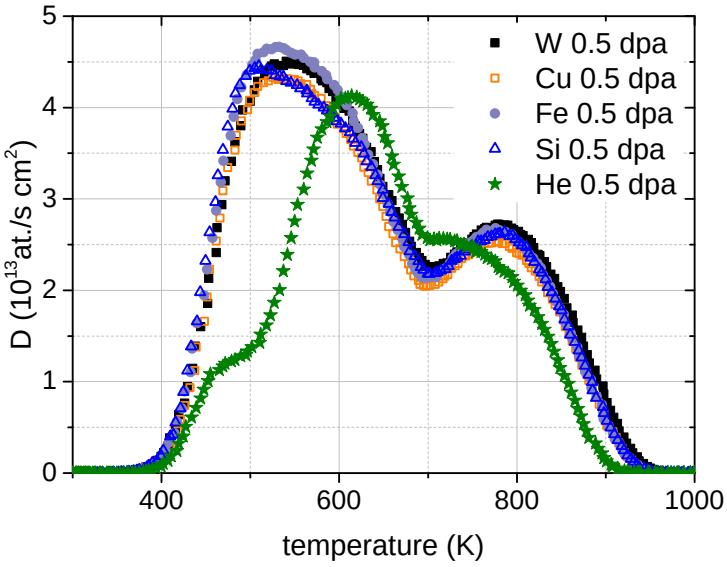

Figure 9: D desorption spectra of tungsten irradiated by medium- to high-mass ions (Si, Fe, Cu, W) up to 0.5 dpa. Reproduced from [20] with permission.

D depth profiles (Fig. 7a)). Figure 10 and 11 show the D depth profiles for tungsten damaged by high-mass and medium- to low-mass ions respectively. In Figure 11 the D depth profile of the D 0.04 dpa before D loading in PlaQ is shown. For an easier comparison between the two figures the D depth profile of Si 0.04 dpa is plotted in both. Clear differences in the D depth profiles are observed. Nevertheless, all samples, except H 0.04 dpa, reach a D concentration in the peak of about 0.8 - 1 at.%. Within the 3σ uncertainty, shown as uncertainty band in Fig. 10 and 11 the D concentration in the peak can be considered as similar. In the depth of about 1.3-1.5 μm, where the damage peak maximum is located, the same damage level is reached in every sample, compare Fig. 1. Therefore, a similar D concentra-

tion is expected in this depth region. The H 0.04 dpa shows a significantly lower D retention and will be discussed later. The differences observed in the D depth profiles seem to be a little arbitrary. Especially the peak position in the NRA profiles of Fe 0.04 dpa, Cu 0.04 dpa and Si 0.04 dpa seems to be shifted to smaller depths. Therefore, a consideration of the uncertainties of the NRADC calculation is needed. One reason for the observed differences are the inherent uncertainties of the depth profiles themselves. The uncertainty of the atomic fraction of D in a certain layer system is determined by NRADC [44] in the final MCMC optimization and is shown as 3σ uncertainty band in the depth profiles. But, in addition, uncertainty arises due to the selection of the step widths in the D depth profiles in the NRADC evaluation process. Each layer intervall in the D depth profile represents the average D concentration within this depth intervall. When calculating the most probable layer system describing the measured raw data, NRADC takes into account the depth resolution. The achievable depth resolution from the two proton detectors at 135 ° is in a depth of 1.5 to 2 μm only about 0.4 μm to 0.6 μm, as calculated by ResolNRA [46]. In the depth of 1.5 - 2 μm the damage peak and the sharp drop from the damage peak to zero is found, compare Fig. 1, and possibly the depth resolution is not enough to resolve the D depth profile correctly. To check this, the depth profile of Si 0.04 dpa was recalculated using a slightly different minimal depth resolution in the Markov Chain Sampling. The difference was of about $\pm$ 50 nm. Figure 12 compares the obtained D depth profile with the previous D depth profile which is also shown in Fig. 10. It can be seen that the binning in the depth profile changed significantly. The depth resolution is, hence, not sufficient to correctly resolve the damage peak and the tail of the

damage depth profile. This can be the reason for the differences observed in the evaluated D depth profiles. Hence, for the 0.04 dpa case the detailed form of the D depth profiles is rather uncertain. To get a better depth resolution a detector at higher scattering angle should be used as described in [60], [61]. Unfortunately, the detector at 175° was unavailable at the time of the measurements. The most robust quantity obtained from the depth profiles is the total D amount retained in the sample. This value can be calculated by integrating the evaluated depth profiles.

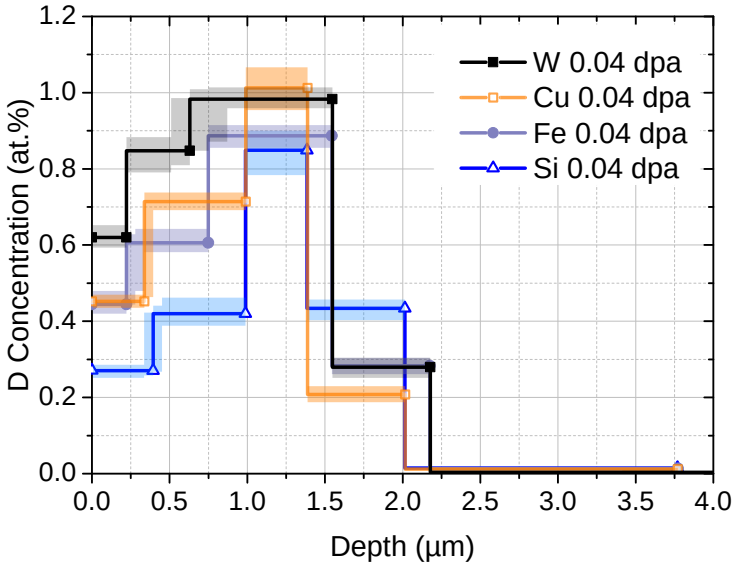

Figure 10: D depth profiles in tungsten irradiated by medium- to high-mass ions (Si, Fe, Cu, W) for 0.04 dpa. The uncertainty bands indicate the 3σ uncertainty. Reproduced from [20] with permission.

The 0.04 dpa damage level represents the increase regime in the D retention behavior, i.e., a higher damage level results in a higher D retention [4, 21, 19].

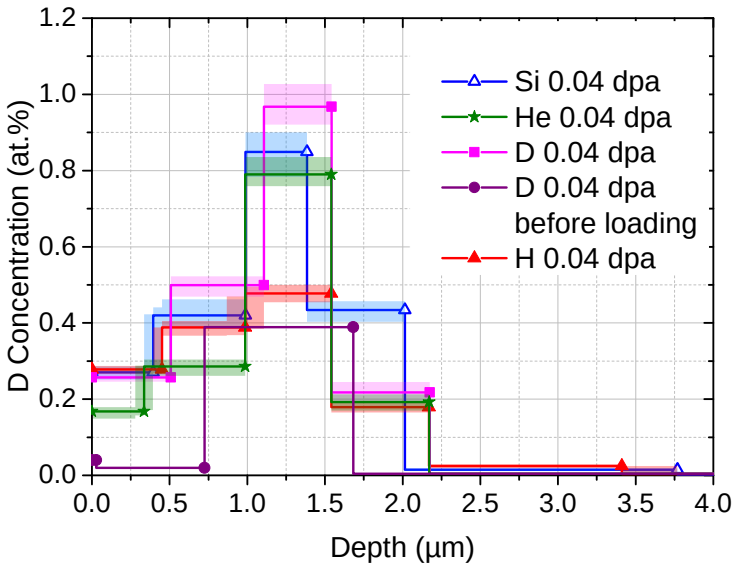

Figure 11: D depth profiles in tungsten irradiated by low to medium-mass ions (H, D, He, Si) for 0.04 dpa. The uncertainty bands indicate the 3σ uncertainty. Reproduced from [20] with permission.

The integral damage level between the different ions is not equal, see Figs. 1 and 6. For comparing the D amount in samples with different integral damage levels the most robust parameter is the number of trapped D atoms per displacement. The NRA D depth profiles and TDS spectra were integrated yielding the total trapped D amount, the integral damage was obtained by integrating the SRIM damage profile. The obtained total D amount was divided by the damage integral giving the number of D atoms per displacement as described in Eq. 2.

$$\frac{D\ integral\ obtained\ from\ NRA}{integrated\ SRIM\ damage\ depth\ profile} = \frac{Number\ of\ D\ atoms}{number\ of\ displacements} \tag{2}$$

The D amount per dpa is listed in Tab. 4. For medium to heavy ion irradiation

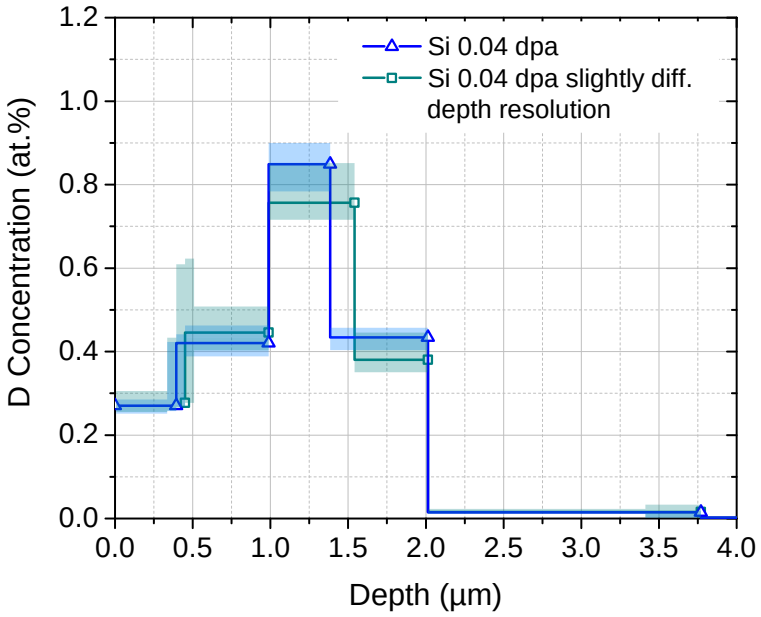

Figure 12: D depth profiles of Si 0.04 dpa samples calculated with slightly different depth resolutions (for further details see text). The uncertainty bands indicate the 3σ uncertainty. Reproduced from [20] with permission.

the variation in the total D amount retained per displacement is below 20%.

Figures 13 and 14 show the obtained normalized D desorption spectra from the samples damaged up to 0.04 dpa. As in the 0.5 dpa case all desorption spectra start and end at the same temperature. As the 0.04 dpa level is in the increase regime the TDS spectra were normalized with the damage integral obtained from the integration of the SRIM damage depth profiles, (see Fig. 6). As in the 0.5 dpa case three desorption peaks are observed in all irradiated samples. The three peaks are located at temperatures of about 480-500 K, 580-600 K and 760-770 K, respectively. The first two peaks are not clearly distinguishable resulting in a broad

D-atoms per displacement

ion	NRA	TDS
W	0.296	0.267
Cu	0.253	0.254
Fe	0.296	0.284
Si	0.303	0.286
He	0.343	0.329
D	0.333	0.330
H	0.239	0.233 (0.527)

Table 4: Total D amount per displacement obtained by NRA and TDS for the 0.04 dpa samples. For H 0.04 dpa a significant amount of hydrogen is retained as protium. The complete hydrogen isotope amount per displacement is given in brackets and is derived from TDS from the sum of the H_2, HD, D_2 signals. For the other samples the total hydrogen amount is equal to the D amount.

peak structure. The first two peaks appear at comparable temperatures as for the 0.5 dpa samples. The third peak apears at somewhat lower temperatures. Figure 13 shows the normalized TDS spectra from tungsten damaged by the medium-mass to high-mass ions. The D desorption spectra are very similar for all four ion irradiations. Hence, the D retention in tungsten damaged by medium- to high-mass ions is also comparable for the 0.04 dpa case. Small differences are observed in the first broad peak structure, due to different peak intensities of the first and second peak. The heights of the broad peak structure are different within 20 %. Figure 14 shows the D desorption spectra obtained from the irradiation with light ions up to 0.04 dpa. For better comparison with Fig. 13 the Si 0.04 dpa spectrum is also plotted. It becomes clear that the D retention in tungsten damaged by light ions is significantly different than for the medium- to high-mass ions. Especially in the broad peak structure of the overlapping peaks 1 and 2 at around 500 K significant differences are observed. On the contrary, the third peak in the desorption

spectra at about 760 K is for all 0.04 dpa samples, beside H 0.04 dpa, very similar. With other words, the D desorption at high temperature (i.e. for T > 700 K) is very similar for the light and medium- to high-mass ions, except H 0.04 dpa. Although sample H 0.04 dpa shows the peak at the same position its intensity is significantly lower. This point will be discussed further below. He 0.04 dpa and D 0.04 dpa show a higher first peak. The total D amount of He 0.04 dpa sample and D 0.04 dpa sample compared with the total D amount of W 0.04 dpa sample is 23 % higher. The higher D retention in the He 0.04 dpa sample can be explained with enhanced hydrogen isotope retention in the helium implantation zone as for the He 0.5 dpa sample. The D desorption spectrum from sample D 0.04 dpa is higher as more D was in the sample due to the preceding D implantation (during damaging with D, as can be seen in the depth profile of Fig. 11). The H 0.04 dpa sample shows a lower D desorption spectrum than all other spectra in Fig. 11. This is in good agreement with the NRA depth profile of H 0.04 dpa which also shows lower D retention compared with D 0.04 dpa.

However, Fig. 14 shows only the D desorption spectra derived from HD and D_2. As tungsten was in this case damaged with protons the full hydrogen isotope desorption spectrum including protium must be considered. Figure 15 shows the complete hydrogen isotope desorption spectrum of H and D, derived from H_2, HD, D_2, for the H 0.04 dpa sample. In addition to the total number of released H isotopes, the individual contributions of H_2, HD, D_2 are also shown. For this sample the H_2 signal and HD signal are clearly not negligible. In the complete hydrogen isotope desorption spectrum the second peak is dominant. In total, the contribution of protium to the total hydrogen release is about 56 % in this sample.

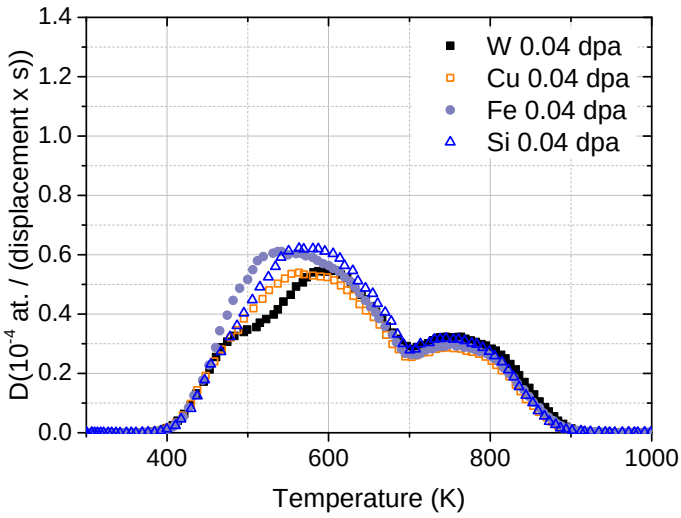

Figure 13: Normalized D desorption spectra from tungsten irradiated by medium- to high-mass ions (Si, Fe, Cu, W) for 0.04 dpa, normalized by the integral damage. Reproduced from [20] with permission.

In Fig. 16 the hydrogen isotope desorption spectrum for D 0.04 dpa sample is shown in the same way. The magenta curve shows the full hydrogen isotope desorption spectrum of D 0.04 dpa which is very similar to the D desorption spectrum already shown in Fig. 14. For this sample the protium signal can be neglected. The H_2 signal is practically invisible and the HD signal is very low. Also for all other investigated samples in this study the contribution of protium from H_2 and HD to the total hydrogen isotope release was negligible. The fact that the H_2 and HD signals are so strong in H 0.04 dpa indicates that the implanted protium got trapped in the created defects. Apparently the D fluence during loading was not enough for full isotope exchange. The significant higher amount of hydrogen isotopes per displacement found in H 0.04 dpa (compare Tab. 4) can be explained

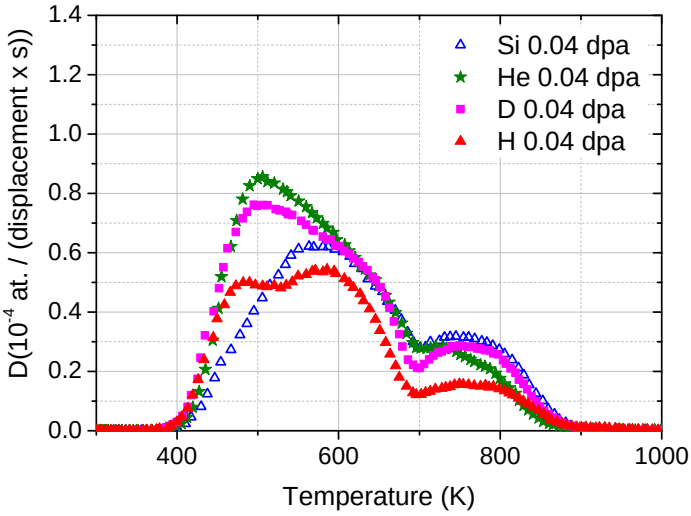

Figure 14: Normalized D desorption spectra of tungsten irradiated by low to medium-mass ions (H, D, He, Si) for 0.04 dpa, normalized by the integral damage. Reproduced from [20] with permission.

by defect stabilization observed in [50]. Markelj et al. [50] showed that the D retention is increased when simultaneously during displacement damage hydrogen isotopes are present. The effect is not observed in the D 0.04 dpa. Note please that the fluence during D irradiation was almost three times lower than during H irradiation, and so was the implanted D concentration, compare Tab. 1. Hence, the defect stabilization effect might be too low to be observed in the D 0.04 dpa sample.

Summarizing, the tungsten samples irradiated by medium (Si) to high-mass ions (Fe, Cu, W) to 0.04 dpa show a comparable D retention per displacement. Tungsten irradiated by light ions (H, D, He) up to 0.04 dpa shows a significant different D retention behavior.

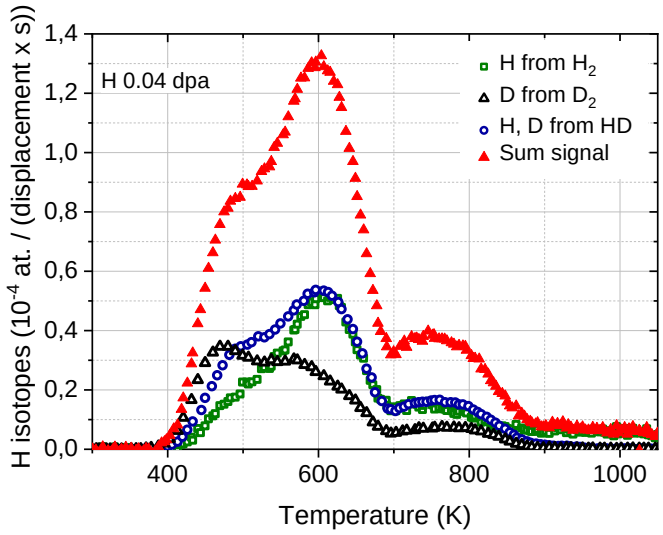

Figure 15: Normalized complete hydrogen isotope desorption spectra (red) for sample H 0.04 dpa obtained from H and D signal from H_2, HD, D_2. Additionally, the components of the signals from H_2, HD, D_2 are shown.

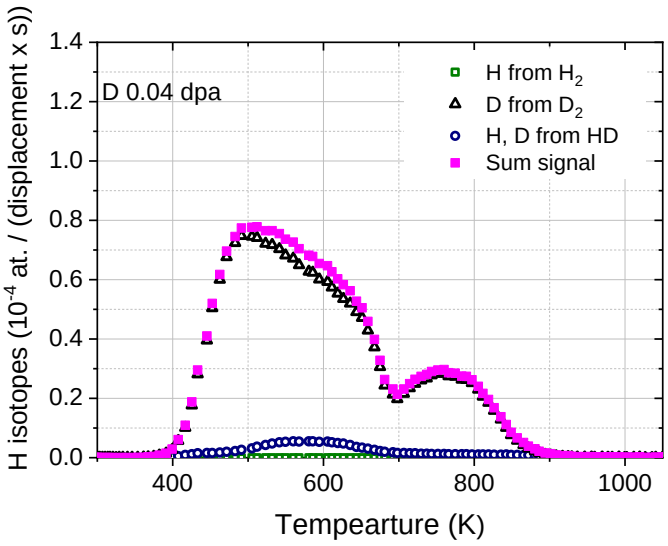

Figure 16: Normalized complete hydrogen isotope desorption spectra (magenta) for sample D 0.04 dpa obtained from H and D signal from H_2, HD, D_2. Additionally, the components of the signals from H_2, HD, D_2 are shown.

5 Summary and Conclusions

This work compared systematically the D retention in tungsten irradiated by different ions. Samples of recrystallized tungsten were damaged with different ion species (H, D, He, Si, Fe, Cu, W) at energies between 0.3 and 20.3 MeV to damage levels of 0.04 dpa and 0.5 dpa in the damage peak maximum. As different ions with different energies were used, the effect of the primary recoil energy spectrum, the effect of different ion species and the effect of different average damage rates on the deuterium uptake was investigated. In order to decorate the created radiation defects with D the samples were exposed to a low-temperature D plasma at 370 K. The D retention was studied by nuclear reaction analysis (NRA) using the D(^{3}He, p)α reaction and by thermal desorption spectroscopy (TDS).

Tungsten damaged by medium- to high-mass ions (Si, Cu, Fe, W) shows very similar D depth profiles and nearly identical deuterium desorption spectra in the 0.5 dpa case. Hence the D retention in tungsten can be considered as identical between medium-mass to high-mass ions in the 0.5 dpa case, which represents the saturation regime. Tungsten irradiated by helium up to 0.5 dpa shows a significantly different D retention: The D depth profile obtained by NRA is more peaked and a higher D concentration is reached in the damage peak maximum. The D desorption spectrum of tungsten irradiated by He up to 0.5 dpa shows three well distinguishable peaks with different intensities and at slightly different temperatures as tungsten irradiated by medium- to high-mass ions. No D saturation effect in this sample was observed. This different D retention behavior is probably due to He bubble formation which serves as additional trapping sites for D.

In the 0.04 dpa case more differences were observed. The 0.04 dpa damage level

represents the increase regime in the D retention behavior of tungsten. In this regime more damage results in a higher D retention. The samples were irradiated with one energy for each ion species to have 0.04 dpa in the damage peak. Due to different widths of the calculated damage distribution, the integral damage over the whole damage depth was different for the different ions. As a consequence, the D retention had to be normalized by the integral damage to allow a meaningful comparison. The differences in the normalized total amounts of retained D obtained from the D depth profiles and desorption spectra are below 20% for medium- to high-mass ion irradiations (Si, Cu, Fe, W). The normalized D desorption spectra are similar for Si, Cu, Fe, W irradiations, beside small differences in the broad desorption peak structure at 550 K. The heights of the broad peak structure consisting of the first two desorption peaks show a difference up to 20%. The third desorption peak is nearly identical. Therefore, it can be stated that the D retention in tungsten irradiated by medium to high-mass ions at 0.04 dpa is similar. For tungsten irradiated by low mass ions (H, D, He) larger differences in the D retention were found. The intensity of the broad peak structure consisting of the first two peaks is significantly higher. The third peak was very similar in all irradiations. The D desorption spectra showing a significant different shape are suggesting a defect structure different from that of the medium to high-mass ions. Because the D retention in tungsten damaged by medium- to high-mass ions (Si, Fe, Cu, W) is nearly identical for 0.5 dpa and similar for 0.04 dpa the results presented here are especially useful for comparing D retention data of tungsten damaged by different ions from different experiments. At damage levels high enough for D retention to saturate, data from medium- to high-mass ion irradiations can

be directly compared. At lower damage levels, more caution is needed. If identical integral dpa values are used, a similar D retention can be expected from the irradiation by medium- to high-mass ions.

Heavy ion irradiation is often used for simulating the displacement damage created by 14 MeV neutrons. This is justified by the fact that neutrons produce similar large dense cascades in tungsten as heavy ions. However, there are significant differences of primary recoil energies between 14 MeV neutron irradiation and heavy ion irradiation. The maximum recoil energy of a tungsten atom after a head on collision with a 14 MeV neutron is about 290 keV, while the maximum primary recoil energies ranged from 3.5 MeV in Si irradiation to 20.3 MeV in W irradiation in this study. Nevertheless, despite the differences in the recoil energy spectra the D retention was identical in the high dpa case for medium-mass to high-mass ions (Si, Fe, Cu, W). No dependence of the primary recoil energy spectrum on the D retention was found. This can be explained by the fact that cascades from recoils with energies higher than 150 keV tend to split into individual subcascades, with energies typically below 200 keV [62]. Hence, the high-energy tail of the recoil distribution produces similar types of defects. Molecular dynamics simulations have shown that these energetic cascades frequently produce very large defect clusters [63]. The subcascade splitting also explains why the samples irradiated with different heavy ions show similar D retention. For the H, D and He irradiations, on the other hand, recoil energies never come close to 150 keV, and hence, the athermal formation of large clusters in the primary damage is much less frequent. The above considerations suggest that the neutron irradiation of tungsten in a future fusion reactor will result in a similar D retention as in tungsten damaged by high-mass

ions. Hence, the use of heavy ions to simulate displacement damage by neutrons seems justified.

Acknowledgment

This work has been carried out within the framework of the EUROfusion Consortium and has received funding from the Euratom research and training programme 2014-2018 and 2019-2020 under grant agreement No 633053. The views and opinions expressed herein do not necessarily reflect those of the European Commission. AES acknowledges support from the Academy of Finland through project No. 311472. The technical assistance with ion beam measurements by J. Dorner and M. Fußeder is gratefully acknowledged.

References

[1] Y. Hirooka et al., Journal of Nuclear Materials **196-198**, 149 (1992).

[2] D. Naujoks et al., Nuclear Fusion **36**, 671 (1996).

[3] M. t Hoen et al., Nuclear Fusion **52**, 023008 (2012).

[4] B. Tyburska, V. K. Alimov, O. V. Ogorodnikova, K. Schmid, and K. Ertl, Journal of Nuclear Materials **395**, 150 (2009).

[5] O. V. Ogorodnikova, B. Tyburska, V. Alimov, and K. Ertl, Journal of Nuclear Materials **415**, S661 (2011).

[6] J. Roth et al., Journal of Nuclear Materials **390-391**, 1 (2009).

[7] J. Knaster, A. Möslang, and T. Muroga, **12**, 424 (2016).

[8] G. S. Was, *Fundamentals of Radiation Materials Science Metalls and Alloys*, Springer-Verlag Berlin Heidelberg, 2010.

[9] O. Ogorodnikova and V. Gann, Journal of Nuclear Materials **460**, 60 (2015).

[10] P. Vladimirov and S. Bouffard, Comptes Rendus Physique **9**, 303 (2008).

[11] G. M. Wright, M. Mayer, K. Ertl, G. de Saint-Aubin, and J. Rapp, Nuclear Fusion **50**, 075006 (2010).

[12] W. R. Wampler and R. P. Doerner, Nuclear Fusion **49**, 115023 (2009).

[13] M. Fukumoto et al., Journal of Nuclear Materials **390-391**, 572 (2009).

[14] J. F. Ziegler, J. P. Biersack, and M. D. Ziegler, *The Stopping and Range of Ions in Matter*, SRIM co., 2008.

[15] K. H. Nordlund et al., Primary radiation damage in materials review of current understanding and proposed new standard displacement damage model to incorporate in cascade defect production efficiency and mixing effects, OECD Nuclear Energy Agency, 2015.

[16] R. S. Averback and T. Diaz de la Rubia, Materials Science and Engineering **51**, 281 (1997).

[17] Standard practice for neutron radiation damage simulation by charge-particle irradiation, Technical report, ASTM E521-96(2009)e2 ASTM International, West Conshohocken, PA, 2009.

[18] R. E. Stoller et al., Nuclear Instruments and Methods in Physics Research Section B: Beam Interactions with Materials and Atoms **310**, 75 (2013).

[19] V. Alimov et al., Journal of Nuclear Materials **441**, 280 (2013).

[20] B. Wielunska, *Characterization of Radiation Damage in Tungsten*, PhD thesis, Technische Universität München, 2020.

[21] O. Ogorodnikova and V. Gann, Journal of Nuclear Materials **460**, 60 (2015).

[22] T. Schwarz-Selinger, private communication.

[23] K. Nordlund, Computational Materials Science **3**, 448 (1995).

[24] J. F. Ziegler, U. Littmark, and J. P. Biersack, *The stopping and range of ions in solids*, volume p.321, Pergamon New York, 1985.

[25] M. R. Gilbert, J. Marian, and J.-C. Sublet, Journal of Nuclear Materials **467**, 121 (2015).

[26] F. Maury, M. Biget, P. Vajda, A. Lucasson, and P. Lucasson, Radiation Effects **38**, 53 (1978).

[27] T. Schwarz-Selinger, Nuclear Materials and Energy **12**, 683 (2017).

[28] J. Barton, Y. Wang, T. Dittmar, R. Doerner, and G. Tynan, Nuclear Instruments and Methods in Physics Research Section B: Beam Interactions with Materials and Atoms **332**, 275 (2014), 21st International Conference on Ion Beam Analysis.

[29] M. Miyamoto et al., Journal of Nuclear Materials **463**, 333 (2015).

[30] V. Chernikov et al., Journal of Nuclear Materials **212-215**, 375 (1994).

[31] N. Hashimoto et al., Journal of Nuclear Materials **347**, 307 (2005).

[32] V. T. Astrelin et al., Journal of Nuclear Materials **396**, 43 (2010).

[33] N. Enomoto, S. Muto, T. Tanabe, J. Davis, and A. Haasz, Journal of Nuclear Materials **385**, 606 (2009).

[34] W. Wang, J. Roth, S. Lindig, and C. Wu, Journal of Nuclear Materials **299**, 124 (2001).

[35] PLANSEE Metall GmbH - High Perfomance Materials, Austria.

[36] A. Manhard, G. Matern, and M. Balden, Practical Metallography **50**, 5 (2013).

[37] A. Manhard, M. Balden, and S. Elgeti, Practical Metallography **52**, 437 (2015).

[38] A. Manhard, T. Schwarz-Selinger, and W. Jacob, Plasma Sources Science and Technology **20**, 015010 (2011).

[39] S. Kapser et al., Nuclear Fusion **58**, 056027 (2018).

[40] T. Schwarz-Selinger, J. Bauer, S. Elgeti, and S. Markelj, Nuclear Materials and Energy **17**, 228 (2018).

[41] J. Bauer et al., Nuclear Fusion **57**, 086015 (2017).

[42] M. Mayer, E. Gauthier, K. Sugiyama, and U. von Toussaint, Nuclear Instruments and Methods in Physics Research Section B **267**, 506 (2009).

[43] M. Mayer, *SIMNRA User's guide*, Tech. Rep. IPP 9/113. Garching: Max-Planck-Institut fur Plasmaphysik, 1997.

[44] K. Schmid and U. von Toussaint, Nuclear Instruments and Methods in Physics Research Section B: Beam Interactions with Materials and Atoms **281**, 64 (2012).

[45] B. Wielunska, M. Mayer, T. Schwarz-Selinger, U. von Toussaint, and J. Bauer, Nuclear Instruments and Methods in Physics Research Section B: Beam Interactions with Materials and Atoms **371**, 41 (2016).

[46] M. Mayer, Nuclear Instruments and Methods in Physics Research Section B: Beam Interactions with Materials and Atoms **266**, 1852 (2008).

[47] S. Kapser, *Deuterium Permeation Through Tungsten Driven by Plasma-Based Low-Energy Ion Implantation*, PhD thesis, Technische Universtät München, Fakultät für Physik, 2018.

[48] M. Zibrov et al., Nuclear Fusion **59**, 106056 (2019).

[49] E. Salançon, T. Dürbeck, T. Schwarz-Selinger, F. Genoese, and W. Jacob, Journal of Nuclear Materials **376**, 160 (2008).

[50] S. Markelj et al., Nuclear Fusion **59**, 086050 (2019).

[51] A. Manhard, K. Schmid, M. Balden, and W. Jacob, Journal of Nuclear Materials **415**, S632 (2011).

[52] M. Balden, A. Manhard, and S. Elgeti, Journal of Nuclear Materials **452**, 248 (2014).

[53] S. Markelj, T. Schwarz-Selinger, and A. Založnik, Nuclear Fusion **57**, 064002 (2017).

[54] N. Juslin and B. D. Wirth, Journal of Nuclear Materials **438**, S1221 (2013).

[55] M. Zibrov, S. Ryabtsev, Y. Gasparyan, and A. Pisarev, Journal of Nuclear Materials **477**, 292 (2016).

[56] S. Ryabtsev, Y. Gasparyan, M. Zibrov, A. Shubina, and A. Pisarev, Nuclear Instruments and Methods in Physics Research Section B: Beam Interactions with Materials and Atoms **382**, 101 (2016).

[57] S. B. Gilliam et al., Journal of Nuclear Materials **347**, 289 (2005).

[58] A. Debelle et al., Journal of Nuclear Materials **362**, 181 (2007).

[59] L. C. Barbara Wielunska, Tomasz Plocinski, in preparation (2020).

[60] B. Wielunska, M. Mayer, and T. Schwarz-Selinger, Nuclear Instruments and Methods in Physics Research Section B: Beam Interactions with Materials and Atoms **387**, 103 (2016).

[61] B. Wielunska, M. Mayer, and T. Schwarz-Selinger, Nuclear Instruments and Methods in Physics Research Section B: Beam Interactions with Materials and Atoms **440**, 202 (2019).

[62] A. D. Backer et al., EPL (Europhysics Letters) **115**, 26001 (2016).

[63] A. E. Sand, S. L. Dudarev, and K. Nordlund, EPL (Europhysics Letters) **103**, 46003 (2013).